THE JOURNAL OF BIOLOGICAL CHEMISTRY VOL. 287, NO. 50, pp. 41888–41902, December 7, 2012

Ablation of Neuronal Ceramide Synthase 1 in Mice Decreases Ganglioside Levels and Expression of Myelin-associated Glycoprotein in Oligodendrocytes*[S]

Received for publication, August 24, 2012, and in revised form, October 12, 2012 Published, JBC Papers in Press, October 16, 2012, DOI 10.1074/jbc.M112.413500

Christina Ginkel[‡], Dieter Hartmann[§], Katharina vom Dorp[¶], Armin Zlomuzica[‖], Hany Farwanah[**], Matthias Eckhardt[‡‡], Roger Sandhoff[§§], Joachim Degen[‡], Mariona Rabionet[§§], Ekrem Dere[¶¶], Peter Dörmann[¶], Konrad Sandhoff[**], and Klaus Willecke[‡1]

From the [‡]Molecular Genetics and [**]Membrane Biology and Lipid Biochemistry, Life and Medical Sciences Institute, [§]Division of Neuroanatomy, Institute of Anatomy, and Institutes of [¶]Molecular Physiology and Biotechnology of Plants and [‡‡]Biochemistry and Molecular Biology, University of Bonn, 53115 Bonn, Germany, [‖]Department of Clinical Psychology and Psychotherapy, Ruhr University, 44780 Bochum, Germany, [§§]Lipid Pathobiochemistry Group within Cellular and Molecular Pathology, German Cancer Research Center, 69120 Heidelberg, Germany, and [¶¶]Université Pierre et Marie Curie (Paris 6), Unité de Formation et de Recherche des Sciences de la Vie, 75005 Paris, France

Background: Ceramide synthase 1 catalyzes the synthesis of C18 ceramide and is mainly expressed in neurons of the brain.
Results: Ablation of ceramide synthase 1 decreases ganglioside levels and expression of oligodendrocytic myelin-associated glycoprotein in motor-impaired mice.
Conclusion: CerS1-derived C18 gangliosides are essential for cerebellar development and neurodevelopmentally regulated behavior in mice.
Significance: Neuronal gangliosides regulate expression of myelin-associated glycoprotein in oligodendrocytes.

Ceramide synthase 1 (CerS1) catalyzes the synthesis of C18 ceramide and is mainly expressed in the brain. Custom-made antibodies to a peptide from the C-terminal region of the mouse CerS1 protein yielded specific immunosignals in neurons but no other cell types of wild type brain, but the CerS1 protein was not detected in CerS1-deficient mouse brains. To elucidate the biological function of CerS1-derived sphingolipids in the brain, we generated CerS1-deficient mice by introducing a targeted mutation into the coding region of the *cers1* gene. General deficiency of CerS1 in mice caused a foliation defect, progressive shrinkage, and neuronal apoptosis in the cerebellum. Mass spectrometric analyses revealed up to 60% decreased levels of gangliosides in cerebellum and forebrain. Expression of myelin-associated glycoprotein was also decreased by about 60% in cerebellum and forebrain, suggesting that interaction and stabilization of oligodendrocytic myelin-associated glycoprotein by neuronal gangliosides is due to the C18 acyl membrane anchor of CerS1-derived precursor ceramides. A behavioral analysis of CerS1-deficient mice yielded functional deficits including impaired exploration of novel objects, locomotion, and motor coordination. Our results reveal an essential function of CerS1-derived ceramide in the regulation of cerebellar development and neurodevelopmentally regulated behavior.

Ceramides and their sphingolipid derivatives have a wide range of biological functions. They have been suggested to play a role in the regulation of cell growth, differentiation, apoptosis, and skin barrier (1, 2). They can also act as receptors for proteins, antibodies, bacteria, and viruses (3, 4). Ceramide consists of a long chain base linked to a fatty acid residue via an amide bond. The chain length of the fatty acid residue can vary between C14 and C36 and can differ in regard to the extent of desaturation or hydroxylation (5, 6). Three different biochemical pathways exist for the production of ceramide, *i.e. de novo* biosynthesis, the sphingomyelinase pathway, and the salvage pathway (4). The *de novo* synthesis of ceramide is initiated at the cytoplasmic face of the endoplasmic reticulum by condensation of serine and palmitoyl-CoA to yield 3-ketosphinganine, which is subsequently reduced to dihydrosphingosine. This can be acylated to dihydroceramide and desaturated to yield ceramide. In the salvage pathway, glycosphingolipids and sphingomyelin are degraded in lysosomes to yield sphingosine, which, like dihydrosphingosine, can be acylated in the endoplasmic reticulum by ceramide synthases (4, 5).

Ceramide synthases (CerS)[2] form a protein family of six members designated CerS1–6. They are transmembrane proteins located in the endoplasmic reticulum. Their nucleotide sequences are largely conserved in eukaryotes (7, 8). CerS1–6

* This work was supported by the German Research Foundation through Collaborative Research Center Grant SFB645, project B2 (to K. W.), project B8 (to P. D.), and project B5 (to M. E.), and through Grant DE1149/5-1 (to E. D.).
[S] This article contains supplemental Figs. S1–S4 and Table S1.
[1] To whom correspondence should be addressed: Life and Medical Sciences Inst., Molecular Genetics, University of Bonn, Carl-Troll-Str. 31, D-53115 Bonn, Germany. Tel.: 49-22873-62743; Fax: 49-22873-62642; E-mail: k.willecke@uni-bonn.de.

[2] The abbreviations used are: CerS, ceramide synthase; MAG, myelin-associated glycoprotein; GD1a, NeuAc(α2–3)Gal(β1–3)GalNAc(β1–4)[NeuAc(α2–3)]Gal(β1–4)Glcβ1-ceramide; GT1b, NeuAc(α2–3)Gal(β1-3)GalNAc(β1–4)[NeuAc(α2–8)NeuAc(α2–3)]Gal(β1–4)Glcβ1-ceramide; BAC, bacterial artificial chromosome; FRT/*frt*, Flp recognition target; LCB, long chain base; LCB-P, LCB phosphate; GDF1, growth and differentiation factor 1; eGFP, enhanced green fluorescent protein; SM4, Gal-3-sulfateβ(1–1)-ceramide; GD1b, Gal(β1–3)GalNAc(β1–4)[NeuAc(α2–8)NeuAc(α2–3)]Gal(β1–4)Glc-ceramide; GM1, Gal(β1–3)GalNAc(β1–4)[NeuAc(α2–3)]Gal(β1–4)Glc(β1–1)-ceramide; GM3, NeuAc(α 2,3)Gal(β1,4)Glc-ceramide; *df*, degrees of freedom.

proteins carry the TLC (Tram-lag1-CLN8) domain, which includes the lag1 domain important for the catalytic activity of ceramide synthases. This domain harbors a C-terminal region including 52 amino acid residues exclusively found in CerS-homologous proteins (9). Previous studies have described point mutations inside the lag1 domain that lead to a loss of function of the CerS1 and CerS5 proteins, respectively. The CerS proteins differ from each other by their substrate specificity toward the length of fatty acyl-CoAs and by their expression pattern in different organs or cell types.

Ceramide can be converted into more complex sphingolipids by attachment of different polar headgroups at its primary alcohol group (C1-OH). Depending on the type of polar group, two major classes, phosphosphingolipids and glycosphingolipids, are defined. The typical phosphosphingolipid in mammalian cells is sphingomyelin, which is synthesized by the transfer of the phosphorylcholine moiety (from phosphatidylcholine) to the C1-OH of ceramide. In an alternative pathway, ceramide can be modified by the addition of one or more sugar moieties. Many variations of glycosphingolipids exist. Usually glucose or galactose residues are attached to ceramide, resulting in glucosylceramide and galactosylceramide, respectively. The sulfuric acid esters of galactosylceramide are designated as sulfatides. Additionally, galactose can be transferred to glucosylceramide to form lactosylceramide, which plays a pivotal role as a precursor for the synthesis of complex glycosphingolipids, *e.g.* gangliosides (5, 10). Gangliosides play an important role in the development and physiology of the brain (11). As compared with astrocytes and oligodendrocytes, postmitotic neurons express particularly high levels of complex gangliosides (12). Gangliosides can serve as interaction molecules for surface proteins, *e.g.* myelin-associated glycoprotein (MAG) in oligodendrocytes (13). MAG is expressed on the inner myelin sheath directly apposed to the axon surface and has been shown to bind to gangliosides GD1a and GT1b located on the neuronal membrane (14).

CerS1 catalyzes the synthesis mainly of C18 ceramide and has been reported to be expressed in neurons of the brain (15–17). Recently, Zhao *et al.* (17) reported the first data on animals bearing a naturally occurring mutation of CerS1, pointing toward specific roles of this enzyme in ceramide biosynthesis in the brain. They found that loss of CerS1 caused progressive Purkinje cell loss in mice and induced accumulation of lipofuscin with ubiquitinated proteins in many brain regions.

In this study, we deleted the catalytic domain of the CerS1 protein in mice. The CerS1$^{-/-}$ mice do not express the CerS1 protein as demonstrated by new specific antibodies. We investigated phenotypic abnormalities in these mutant mice relative to wild type mice. Our study goes beyond the data by Zhao *et al.* (17) insofar as we found that synthesis of gangliosides and expression of ganglioside-associated MAG protein were both significantly decreased in CerS1-deficient mice. Mice lacking the CerS1 protein exhibited a 40% reduced size of the cerebellum. As these animals aged, behavioral deficits appeared in CerS1$^{-/-}$ mice. We provide data on altered sphingolipid levels early after mouse brain development and subsequent postontogenetic life up to early senescence. The comprehensive neurobehavioral studies reported here indicate that the CerS1 protein plays an essential role in the development of normal neural physiology in mice.

MATERIALS AND METHODS

Generation of the CerS1KO Vector—The point mutation in the start codon of *cers1* and insertion of the EcoRI restriction site were generated by PCR mutagenesis, and the resulting fragment was cloned by AgeI/BamHI restriction into the vector, which contained the 5′ region of *cers1* in pBluescript (3.4-kb BamHI/Asp718I fragment from the BAC clone MPMGc121N06760Q4 (Sanger Institute, Cambridge, UK)). Deletion of exon 3 was achieved by PCR mutagenesis with the above mentioned BAC clone DNA and cloning via BamHI/EcoRI restriction of the flanking sites into pBluescript. The stop codon of the *egfp* gene was deleted by PCR mutagenesis, and the resulting DNA was inserted between the flanking sites of exon 3 in the vector described above. Afterwards, the 3′ homologous region including exons 4–6 (1.5-kb EcoRI/PspOMI fragment from the above mentioned BAC clone in pBluescript) was cloned into the vector, which contained the flanking sites of exon 3 and the *egfp* gene. The 5′ homologous region with the point-mutated exon 1 was cloned into this vector by Asp718I/BamHI restriction. Exon 2 was inserted by cloning of the 4.3-kb BamHI fragment of the BAC clone into the vector mentioned above. In the final step, we cloned the neomycin resistance gene, driven by the phosphoglycerate kinase promoter and flanked by *frt* (Flp recognition target) sites into the vector described above. To this end, a 1.9-kb EcoRI/BamHI fragment from the vector IRES-eGFPcre-FRT-kanamycin-FRT (18) was cloned into the SpeI recognition site of intron 1. The final nonconditional CerS1KO vector was analyzed by restriction mapping and partial sequencing (GATC Biotech, Konstanz, Germany). The functionality of the *frt* sites was tested by transformation of the targeting vector into Flp recombinase-expressing *Escherichia coli* bacteria (19).

Screening of Embryonic Stem (ES) Cell Clones—For transfection of HM1 ES cells (20) via electroporation (0.8 kV, 3 microfarads; Gene Pulser, Bio-Rad), 300 μg of DNA of the nonconditional CerS1KO vector were linearized by NotI digestion. Selection of transfected ES cells was carried out with 350 μg/μl G418-neomycin (Invitrogen). Resulting ES cell clones were tested by PCR, analyzing the insertion via the 3′ homologous region. ES cell clones that were positive in PCR analysis were further characterized by Southern blot analyses for recombination at the 3′ and the 5′ homologous regions (external probes) as well as for single integration of the vector construct (internal probe) (data not shown). The transfection of cells yielded 1.6% stably transfected cell clones harboring the vector inserted via homologous recombination into the genome.

Generation of CerS1-mutated Mice—The ES cells were injected into C57BL/6 mouse blastocysts following standard conditions (21). Chimeras were mated with C57BL/6 mice, and the agouti-colored offspring were analyzed for homologous recombination by PCR of tail tip DNA using an intron-specific sense primer (CerS1_1, 5′-ACT CTC TCG GTG TCC ATC TAG-3′), which was combined with a *cers1* intron-specific antisense primer (CerS1_3, 5′-ATG AGT TTC ACC AAC CTG GGC-3′) and *neomycin*-specific antisense primer (CerS1_2,

5′-CAT GCG AAA CGA TCC TCA TCC-3′). After breeding the progeny with Flp recombinase-expressing and wild type mice, we obtained heterozygous and finally homozygous CerS1$^{-/-}$ mice with an 87.5% C57BL/6 background. Mice were kept under standard housing conditions with a 12/12-h dark/light cycle and with standard diet and water *ad libitum*. All mice were raised in accordance with instructions of local and state authorities regarding experiments with animals.

Southern Blot Hybridization—For Southern blot hybridization of wild type (Cers1$^{+/+}$), heterozygous (Cers1$^{+/-}$), and homozygous mice (Cers1$^{-/-}$), genomic DNA was prepared from adult liver and digested with EcoRI. Genomic DNA was fractionated on 0.6% agarose gels by electrophoresis and transferred onto nylon membranes (Hybond^{TM}-N^{+}, Amersham Biosciences). The hybridization was performed using Quick Hyb hybridization solution (Stratagene, La Jolla, CA) at 68 °C and a [^{32}P]dCTP-labeled probe (Hartman Analytic GmbH, Braunschweig, Germany) for 2 h. The probe consists of an 822-bp DNA fragment upstream of exon 1 of the *cers1* gene and upstream of the 5′ homologous region of the insertion site. Membranes were first washed in 2× SSC, 0.1% SDS at 68 °C, 1× SSC, 0.1% SDS at 68 °C, 0.5× SSC, 0.1% SDS at 68 °C, and 0.1× SSC, 0.1% SDS at 68 °C and then exposed to Hyperfilm^{TM} MP film (Amersham Biosciences) at −70 °C using an intensifying screen.

Northern Blot Hybridization—Total RNA from adult brain tissues was collected using TRIzol (Invitrogen) according to the manufacturer's protocol, and 20 μg were separated by electrophoresis (22) and transferred onto Hybond-N nylon membranes (Amersham Biosciences) by capillary diffusion in 20× SSC. The hybridization was performed with Quick Hyb using a 326-bp PCR cDNA fragment of *cers1* including part of the coding region of exon 1 and exon 2. After stripping, the membrane was hybridized with a BamHI/NotI 741-bp fragment of the pMJ green vector (23), which included part of the coding region of the *egfp* gene. The amounts of total RNA on Northern blots were normalized by hybridization to a SacI/BamHI 300-bp fragment of human glyceraldehyde-3-phosphate dehydrogenase (*gapdh*) (24).

Ceramide Synthase Assay—Brain tissue samples of 6-week-old mice were prepared, and ceramide synthase activity was measured as described (25).

Lipid Extraction—Forebrains and cerebella from mice were weighed and homogenized in 2 ml of water using Precellys®24 (Peqlab Biotechnologie GmbH, Erlangen, Germany). Lipids were extracted from this homogenate with 5 ml of methanol and 2.5 ml of chloroform in a homogenous single phase. Extractions were carried out in screw cap tubes (VWR, Darmstadt, Germany), which were placed in a shaking water bath (37 °C) overnight. Afterwards, the tissue pieces were separated by centrifugation, and the solvents were evaporated under a stream of nitrogen. This procedure was repeated twice with 5 ml of chloroform/methanol (1:1, v/v) and 5 ml of chloroform/methanol (2:1, v/v), respectively, to ensure complete lipid extraction. The pooled extracts were then separated into neutral and acidic fractions as described previously (26). Phospholipids, which might disturb the analysis of sphingolipids, were deesterified by mild alkaline hydrolysis for 2 h at 40 °C using 150 μl of 1 M KOH in methanol in 2 ml of chloroform/methanol (1:1, v/v). After cooling, the samples were neutralized utilizing glacial acidic acid. For desalting of lipid extracts, reversed phase chromatography was performed (27). For measurement of free long chain bases, the neutral lipid extracts were separated and purified using a silica column. The lipid extracts were loaded on chloroform-equilibrated silica columns (Strata-1 Silica, 55 μm, 70 Å, 100 mg; Phenomenex, Aschaffenburg, Germany) and washed five times with chloroform to remove all neutral lipids, and long chain bases were eluted with acetone/isopropanol (1:1, v/v) (28).

Nanoelectrospray Ionization-Tandem Mass Spectrometry—Quantification of sphingolipids was carried out using the Agilent 6530 Accurate-Mass Q-TOF LC/MS instrument equipped with a direct infusion chip-based nanospray ion source. The nanospray solvent was chloroform/methanol/300 mM ammonium acetate (300:665:35) (29). Sphingolipids were ionized in the positive mode. Instrument parameters were set as described previously (28). Sphingolipids were quantified using characteristic fragments generated after collision-induced dissociation and normalized to internal standards as described (30–32) with slight modifications. Hexosylceramides were quantified by the neutral loss of their headgroup sugar, ceramides were quantified by a precursor ion scan for the LCB moiety, sphingomyelin was quantified by a precursor ion scan for the phosphocholine headgroup, free LCBs were quantified by the neutral loss of water, and LCB-P was quantified by the neutral loss of the phosphate headgroup. Fragmentation energies were optimized for each class of sphingolipids: hexosylceramides, 20 V; ceramides, 35 V; sphingomyelin, 25 V; LCB, 20 V; LCB-P, 10 V.

Thin Layer Chromatography—For high performance TLC analysis of gangliosides, the acidic lipid extract was dissolved in chloroform/methanol/water (2:1:0.1, v/v). The extracts were applied on high performance TLC plates (20 × 20-cm silica gel 60 plates, Merck) using equal protein amounts per lane (800 μg for forebrain and 1.6 mg for cerebellum samples). The plates were developed in a high performance TLC separating chamber using chloroform/methanol/0.22% $CaCl_2$ in water (55:45:10, v/v/v). After drying, the separated lipid bands were visualized by treatment of the plates with a solution of 10% $CuSO_4$ and 8% H_3PO_4 (w/v) and heating to 180 °C for 15 min. Differences in lipid levels were analyzed using Student's *t* test for unpaired data.

Immunoblot Analyses—Tissues of wild type and CerS1$^{-/-}$ mice were collected in liquid nitrogen and homogenized by Precellys (Peqlab Biotechnologie GmbH) in 1.5 ml of homogenization buffer (7.5 mM Na_2HPO_4, 2.5 mM NaH_2PO_4, 40 mM NaF, 2 mM EDTA, 0.1% SDS, 1% Triton X-100, 0.1% deoxycholate, pH 7.2) supplemented with a protease inhibitor mixture (Roche Applied Science). Homogenates were centrifuged for 5 min, and protein concentrations were determined using the BCA assay (Sigma). 50 μg of each protein lysate in urea buffer (0.04 M Tris-HCl, 9 M urea, 5% SDS (w/v), 1 mM EDTA, 0.01% bromphenol blue (w/v), 5% 2-mercaptoethanol (v/v), pH 6–8) were separated by SDS-PAGE in a 12% gel (a 10% gel for MAG). Proteins were blotted at 100 V for 90 min in transfer buffer (20 mM Tris, 150 mM glycine, pH 8.3) onto Hybond-C Extra nitrocellulose (GE Healthcare). Membranes were blocked

with 5% milk powder in washing buffer (20 mM Tris, pH 8.0, 150 mM NaCl, 0.2% Tween 20) for 1 h and incubated overnight at 4 °C with a 1:1,000 dilution of rabbit CerS1 antibodies (custom-made to a peptide located at the C terminus of the mouse CerS1 (QMRELEDLREYDTLEAQ), Pineda, Berlin, Germany), a 1:1,000 dilution of rabbit anti-MAG (Abcam, Cambridge, UK), a 1:100 dilution of rabbit anti-growth and differentiation factor 1 (GDF1) (EPR5815, Epitomics), or a 1:1,000 dilution of mouse anti-myelin basic protein (MBP) (sc-376995, Santa Cruz Biotechnology). After washing (three times for 10 min) in washing buffer, membranes were incubated for 1 h at room temperature with a 1:10,000 dilution of horseradish peroxidase-conjugated goat anti-rabbit Ig (Dianova) in blocking solution and washed again (three times for 10 min) in washing buffer. For detection of bound antibodies, the SuperSignal West Pico Chemiluminescent detection kit (Pierce) was used. Standardization of immunoblots was performed by using a 1:10,000 dilution of mouse monoclonal GAPDH antibody (MAB174, Millipore, Darmstadt, Germany) or a 1:10,000 dilution of mouse monoclonal Tubulin antibody (T9026, Sigma) in washing buffer containing 5% milk powder for 30 min at room temperature and a 1:10,000 diluted horseradish peroxidase-conjugated goat anti-mouse Ig (Dianova) under the same conditions. Differences in MAG protein levels were analyzed using Student's *t* test for unpaired data.

Histological Investigations—For high resolution light microscopy based upon semithin sections as well as transmission electron microscopy, mice were killed by an overdose of chloroform and then immediately fixed via sequential transcardiac perfusion with 0.1 M Sörensen buffer with 1% procaine HCl and then 6% glutaraldehyde in 0.1 M Sörensen phosphate buffer again with 1% procaine HCl (pH 7.4). Tissues of interest were dissected and postfixed by immersion in the same fixative without procaine at least overnight. After thorough rinsing in phosphate buffer, regions of interest were either directly or after presectioning with a Leica 1200 Vibratome dissected from the tissues and postfixed in 2% OsO_4, dehydrated in a graded series of ethanol, and embedded in Spurr's epoxy resin formula (Serva). Semithin sections were cut at a thickness of 1 μm, heat-mounted on aminosilane-coated slides, and then double stained with toluidine blue and pyronine G. Light microscopic preparations were photographed with a Nikon 90i photomicroscope equipped with a 12-megapixel Nikon RI camera. After evaluation by light microscopy, blocks were trimmed down to regions of interest of about 1 mm^2 and resectioned at 70 nm for routine transmission EM. Sections were mounted on 300 or 100 mesh copper grids, respectively, contrast stained with uranyl acetate and lead citrate, and examined in a 120-kV Zeiss (Jena, Germany) EM 910 electron microscope.

Immunohistochemical Analyses for CerS1—The expression of CerS1 protein in cerebellum was localized by immunohistochemical methods. In brief, unfixed cerebella were frozen in TissueTek OCT embedding medium (Sakura Finetek, Heppenheim, Germany) and sectioned at 12 μm with a cryostat. The sections were fixed in methanol at −20 °C for 20 min and incubated in 10% (v/v) methanol and 0.3% (v/v) H_2O_2 in washing buffer (50 mM Tris, 1.5% NaCl, 0.3% Triton X-100, pH 7.6) for 15 min at room temperature for blocking of endogenous peroxidase activity. After being washed three times in washing buffer and blocked in 4% goat serum and 5% BSA in washing buffer for 1 h, the sections were incubated with CerS1 antibodies at a 1:100 dilution in blocking solution overnight at 4 °C. After washing three times for 5 min in washing buffer, sections were incubated for 1.5 h at room temperature with a 1:500 dilution of horseradish peroxidase-biotin-conjugated goat anti-rabbit (Invitrogen) in blocking solution and washed again three times for 5 min in washing buffer. For detection of the bound antibodies, the VECTASTAIN Elite ABC kit (Vector Laboratories, Burlingame, CA) was used followed by staining with the VECTOR NovaRED Peroxidase Substrate kit (Vector Laboratories).

Immunofluorescence Analysis—Cerebella were frozen unfixed in TissueTek OCT embedding medium (Sakura Finetek) and sectioned at 12 μm with a cryostat. The sections were fixed in methanol at −20 °C for 20 min. After washing three times for 5 min in washing buffer (50 mM Tris, 1.5% NaCl, 0.3% Triton X-100, pH 7.6) sections were blocked with 5% goat serum in washing buffer for 30 min and incubated overnight at 4 °C with a 1:100 dilution of rabbit CerS1 antibodies, a 1:100 dilution of mouse calbindin antibodies (Sigma), or a 1:500 dilution of mouse NeuN antibody (MAB377, Chemicon, Billerica, MA) in blocking solution. After washing three times for 5 min in washing buffer, sections were incubated for 1.5 h at room temperature with a 1:1,000 dilution of combinations of Alexa Flour 488 and Alexa Fluor 562 secondary antibodies (Invitrogen) in blocking solution and washed again three times for 5 min in washing buffer. TUNEL assays were performed using the *In Situ* Cell Death Detection kit according to the manufacturer's instructions (Roche Applied Science). Sections were mounted with Glycergel mounting medium (Dako, Glostrup, Denmark) and viewed with a laser scanning microscope (Zeiss).

Behavioral Analysis—Seven $CerS1^{-/-}$ (80 ± 13 days old upon arrival in the behavior laboratory) and eight $CerS1^{+/+}$ (68 ± 8 days old upon arrival in the behavior laboratory) male mice with an 87.5% C57BL/6 background were used for behavioral experiments. The mice were acclimatized to the housing conditions for 3 weeks before the behavioral experiments were initiated. During the acclimatization period, animals were left undisturbed in their home cages except for being placed into a clean cage with fresh bedding material once per week. Animals were maintained under a reversed 12-h light/dark cycle with lights on at 7:00 a.m. They had free access to water and standard diet. They were housed in Makrolon cages placed into a ventilated, temperature- and humidity-controlled cabinet (UniProtect, Ehret, Germany). The animals were not handled except to place them into the behavioral apparatuses and back to their home cage after the tests. During these transfers, the mouse was gently picked up by the tail and immediately released into the apparatus or home cage to minimize handling-induced stress. Studies were approved by the local animal ethics committee and the state authorities of North Rhine-Westphalia.

Open Field—Spontaneous exploratory behavior and behavioral habituation were investigated using the open field test (33). Each mouse was given three trials of 10-min duration in the open field with an intertrial interval of 24 h. The open field (30 × 30 × 40 cm) was made of gray *polyvinyl chloride*. It was

placed in a sound-attenuated experimental chamber. A video camera was mounted 40 cm above the open field. A 100-watt white light bulb provided a light density of approximately 20 lux at the center. Open field trials were analyzed offline using the EthoVision tracking system (Noldus, Netherlands). The following variables were measured: (i) locomotion, the distance in cm an animal moved; (ii) center time, the time spent in the center (10 × 10 cm); (iii) corner time, the time spent in the four corners (10 × 10 cm each); and (iv) running speed, the mean running speed (cm/s) in the center or the entire open field.

Repeated exposures to the same open field induce behavioral habituation indicated by low levels of exploratory behavior. Exploratory behavior (dishabituation) can be reinitiated by the introduction of novel stimuli into the familiar open field (34). Twenty hours after the third trial, the mice received a fourth trial in the open field. The experimental procedure was identical to the previous three trials except that visual cues had been attached to the north and south wall of the open field. Additionally, the illumination strength in the center was reduced from 20 to 10 lux. Dishabituation indices for the variables locomotion and mean running speed were calculated as follows: dh = behavior on trial 4/(behavior on trial 3 + trial 4). High index scores close to 1 indicate high behavioral dishabituation, whereas low index scores near 0 would indicate low behavioral dishabituation.

Motor Coordination Learning—Motor coordination and balancing performance were tested with an accelerating rotarod (TSE Systems, Germany). The rod had an axis diameter of 3.5 cm and a striated surface made of black rubber. Each mouse was given three trials per day for 3 consecutive days. Two weeks later, the animals were subjected to three more trials. Each animal was individually placed on the inactive drum, which thereafter was accelerated to a speed of 40 rpm over a period of 5 min. The duration (s) of active performance was registered on each trial. Each trial ended when the mouse fell off the drum or after 5 min.

Vertical Pole Test—A pole wrapped with cord (2-cm diameter, 80-cm length) and bordered at its base by a platform was positioned vertically. The mouse was placed with its forelimbs on the pole and its head facing upward. The latency to perform a 180° turn to face the platform and the total time required to climb down the pole and enter the platform were measured two times with an intertrial interval of 30 min. Each trial lasted for a maximum of 120 s. Incidents of falling, slipping, reclimbs, and back turns were also scored.

Horizontal Wire Test—Each mouse was lifted from the tail and carefully lowered to the middle of a horizontally clamped wire (1 mm in diameter, 90 cm long, lifted 20 cm from the floor) that connected two platforms (4 × 4 cm). The animal was allowed to grasp the wire with its forepaws and to climb to one of the two platforms. The time the mouse needed to reach one of the platforms was recorded during two trials with an intertrial interval of 30–45 min. Horizontal wire test performance (see supplemental Table S1) was scored as described previously (35). A trial was terminated after an animal reached one of the platforms or if 180 s had elapsed.

Spontaneous Alternation in the Y-maze—Spontaneous alternation performance was assessed according to a previous publication (36). The Y-maze had an open roof and was constructed of black Plexiglas with three arms (7.5 cm wide × 18 cm long × 23.5 cm high) radiating from a triangle-shaped central platform. One of the arms differed from the others by a colored rectangular cue inserted at the end of the wall. It was placed in a sound-attenuated experimental chamber. The mouse was placed on the central platform and was allowed to explore the arms of the Y-maze for 5 min. An arm entry was scored when the mouse entered an arm with all four paws. The following parameters were calculated: (i) total number of entries; (ii) number of triplets, the number of consecutive choices of each of the three arms without re-entries during the last three choices and irrespective of the order of the chosen arms; and (iii) alternation ratio, the number of triplets divided by the total number of entries minus 2 (36).

Novel Object Exploration Test—Each animal was allowed to freely explore two copies of a novel object placed into two randomly selected corners of a familiar open field (37, 38). Objects were made of plastic, had a textured surface, and had a height of 18 cm. The time spent exploring the objects (s), the frequency of object contacts, and the total distance moved in cm were scored offline by using an automated tracking device (EthoVision). The automated and unbiased analysis of exploratory behavior in the novel object exploration paradigm was based on a multiple point tracking technique for the identification of the body point center, nose point, and tail base point of an animal. Exploration and contact with an object was assumed when the mouse approached the object zone with its nose with the nose point being within 2 cm of the object border.

Statistics—Spontaneous spatial alternation, open field, and rotarod data are expressed as mean ± S.E. Vertical pole test and horizontal wire data are expressed as medians (with interquartile ranges). The Mann-Whitney *U* test was used for genotype comparisons of pole and horizontal wire test performance. Within-group differences between the first and second trials were calculated by the Wilcoxon test. Open field and rotarod data were analyzed by repeated measures analysis of variance. Long term motor memory was analyzed by Student's *t* tests for paired data. Genotype differences in dishabituation, spontaneous spatial alternation, and novel object exploration were analyzed by Student's *t* test for unpaired data. To determine whether spatial alternation ratios were significantly different from chance level, single group *t* tests against a chance level of 0.5 were performed. Results were considered significant if p values smaller than 0.05 were obtained.

RESULTS

Generation of CerS1$^{-/-}$ Mice—The mouse *cers1* gene is located on chromosome 8 upstream and in close proximity to the gene coding for GDF1 with which it is expressed on the same (bicistronic) mRNA. Both genes together are encoded by eight exons. Deletion of the *gdf1* gene leads to embryonic lethality in mice (39). To prevent that the deletion of *cers1* disturbs the expression of GDF1, we deleted the translational start codon of *cers1* in the first exon and other potential reinitiating start codons in exon 3 together with part of the functional lag1 motif. Instead of the deleted part of exon 3 (amino acid residues 182–191), we introduced a new AUG start codon followed by

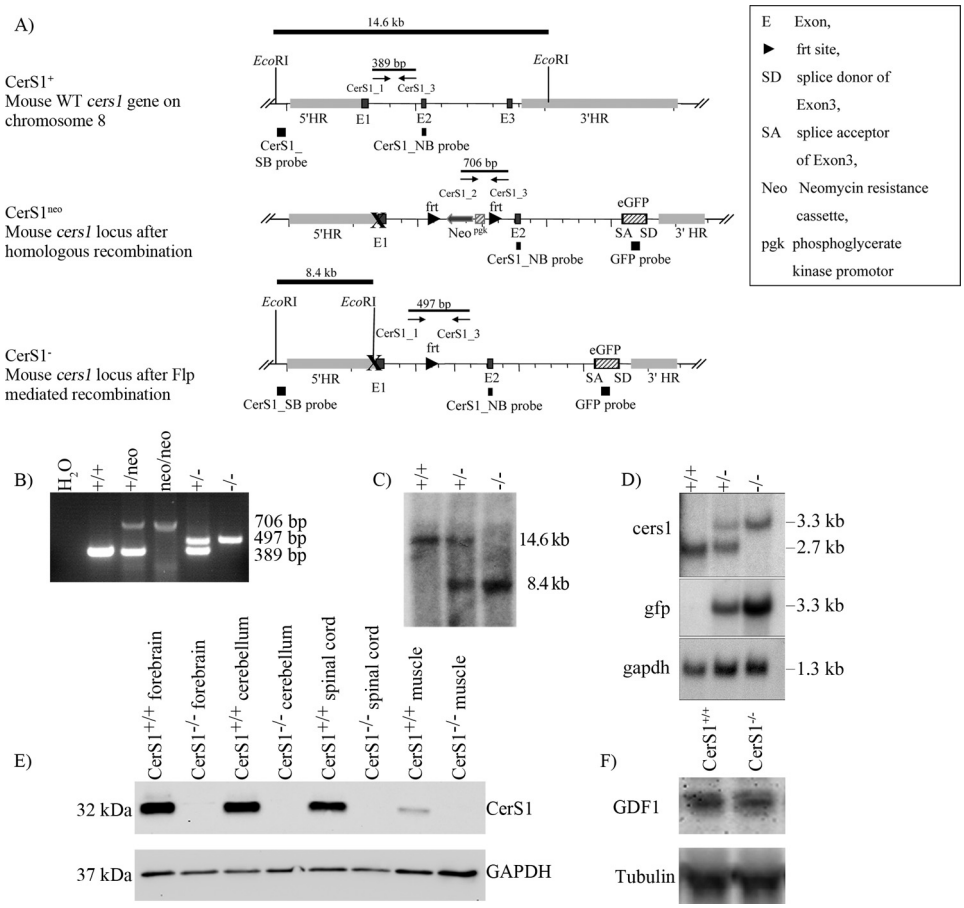

FIGURE 1. **Generation of CerS1$^{-/-}$ mice.** *A*, scheme of the strategy used for the generation of CerS1$^{-/-}$ mice including *cers1* wild type locus, *cers1* locus after homologous recombination (CerS1^{neo}), and *cers1* locus after Flp-mediated recombination (CerS1^{-}). *B*, PCR analysis using genomic tail DNA from mice of all genotypes obtained. The *cers1*-specific primer combination resulted in a 389-bp amplicon for the *cers1* wild type allele, a 706-bp amplicon for the cers1 mutated allele containing the neomycin resistance cassette (*neo*) and a 497-bp amplicon for the *cers1*-mutated allele without the neomycin cassette. *C*, Southern blot analysis of the *cers1* locus demonstrating the homologous recombination of the targeted allele and the generation of the *cers1*$^{-/-}$ allele. After EcoRI digestion, bands corresponding to DNA fragments of the 5′ homology region of wild type and knock-out alleles were detected at 14.6 and 8.4 kb, respectively. *D*, Northern blot analysis of CerS1$^{+/+}$, CerS1$^{+/-}$, and CerS1$^{-/-}$ RNA isolated from whole brain lysates. The CerS1_NB probe detected a transcript of 2.7 kb length for the wild type allele and for the *cers1*-mutated allele a transcript of 3.3 kb length. The *egfp* probe detects also the 3.3 kb transcript for the mutated allele. The *gapdh* probe was used as a loading control. *E*, immunoblot analysis. The CerS1 antibodies recognize a signal of about 32 kDa only in wild type forebrain, cerebellum, spinal cord, and muscle. In CerS1 mutant tissues, no specific signals were found. *F*, immunoblot analysis. A GDF1 antibody recognizes the GDF1 protein in lysates of embryonic day 10 wild type as well as CerS1-deficient animals. *SB*, Southern blot; *NB*, Northern blot; *HR*, homologous region.

the coding DNA of the enhanced green fluorescent protein (eGFP). The *egfp* cDNA was cloned without the translational stop codon so that a fusion protein of eGFP and the remaining part of CerS1 could be translated. The remaining part of CerS1 hypothetically consists of only two transmembrane regions and is expected to be enzymatically inactive as point mutation studies have shown (9). Successful expression of this eGFP-CerS1^{ct} fusion protein should terminate translation of the mutated *cers1* gene at the same stop codon as wild type *cers1*. Thus, the expression of the *gdf1* gene should not be influenced in the CerS1-deficient mice.

For inactivation of the mouse *cers1* gene, we used the non-conditional CerS1KO vector (Fig. 1*A*). After transfection into HM1 ES cells, homologous recombined ES cells were used to generate germ-line transmission chimeras. GFP should be expressed as a fusion protein with the C-terminal peptide of CerS1 (eGFP-CerS1^{ct} fusion protein). However, no GFP signal could be detected via endogenous fluorescence or via detection with antibodies to GFP. This might be due to instability of the eGFP-CerS1^{ct} fusion protein.

Characterization of CerS1$^{-/-}$ Mice—Heterozygous animals without the neomycin selection cassette were used for the generation of a CerS1$^{-/-}$ mouse line with at least 87.5% C57BL/6 genetic background. The homozygous CerS1$^{-/-}$ mice were viable and fertile. Via immunoblot analysis of embryos on embryonic day 10, we detected GDF1 protein in CerS1-deficient animals at the same amount as in embryos of wild type animals (Fig. 1*F*), indicating that the knock-out of CerS1 had not inactivated the second reading frame on the *cers1* mRNA that codes for GDF1. If the second reading frame had been inactivated, embryonic lethality would have resulted.

The different genotypes were confirmed by PCR genotyping (Fig. 1*B*) and Southern blot hybridization (Fig. 1*C*). Offspring of matings with heterozygote CerS1$^{+/-}$ mice were born with the expected Mendelian ratio, indicating a non-essential role of CerS1 during embryogenesis. Northern blot analyses hybrid-

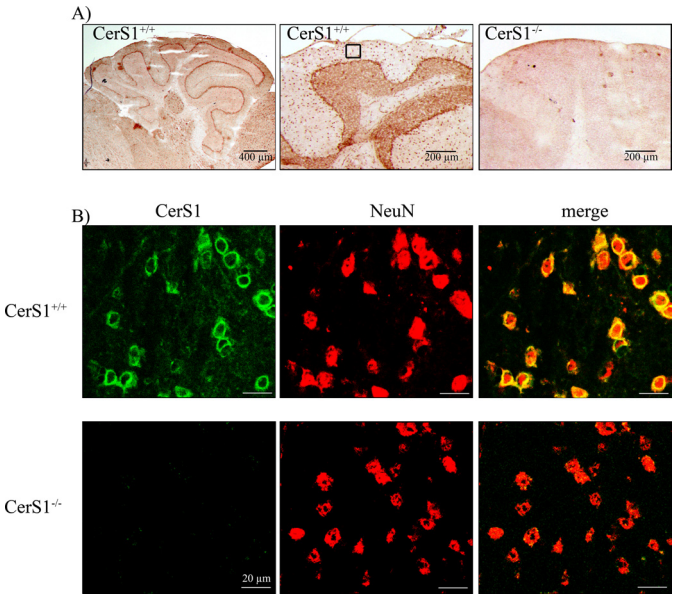

FIGURE 2. **Immunohistochemistry of CerS1 protein in mouse cerebellum.** CerS1 is located in neuronal cells in the cerebellum. *A*, immunoreactivity of CerS1 in sections of wild type and homozygous CerS1$^{-/-}$ cerebella. *B*, presence of CerS1 (*green*) in NeuN-positive (*red*) cells in sections of wild type and homozygous CerS1$^{-/-}$ cerebella. Immunofluorescence analyses were performed within the region of the highlighted *box* in *A*.

ized with a *cers1* probe showed a 2.7-kb transcript for wild type and a 3.3-kb transcript for the mutated genotype. With the *gfp* probe, the 3.3-kb transcript was found only in the mutated genotype (Fig. 1*D*).

Generation of CerS1 Antibodies—GFP should have been expressed as a fusion protein with the C-terminal peptide of CerS1 (eGFP-CerS1^{ct} fusion protein); however, no GFP signal could be detected via endogenous fluorescence or via detection with antibodies to GFP. To detect the CerS1 protein, we generated peptide antibodies against a peptide located in the C-terminal part of CerS1. These antibodies should detect wild type CerS1 and the eGFP-CerS1^{ct} fusion protein in the mutated CerS1 mice. In Western blot analysis, CerS1$^{+/+}$ tissue showed a signal in forebrain, cerebellum, spinal cord, and muscle at about 32 kDa (Fig. 1*E*). No signal could be detected in CerS1$^{-/-}$ tissue, indicating that the eGFP-CerS1^{ct} fusion protein is not expressed or is rapidly degraded. The specificity of the CerS1 antibodies was checked by immunoblot analysis of lysates of CerS1-overexpressing and wild type HEK-293 cells (supplemental Fig. S1).

Localization of CerS1 Expression—To analyze the localization of CerS1 protein, we performed immunostainings with newly generated CerS1 antibodies. Immunohistochemical stainings showed a strong expression of CerS1 in different cerebellar regions (Fig. 2*A*). In immunofluorescence analyses, we found perinuclear signals in cerebellum (Fig. 2), spinal cord, and eye (not shown) only in neurons of CerS1$^{+/+}$, but not of CerS1$^{-/-}$, mice as verified by its co-expression with NeuN, a marker for neuronal nuclei (Fig. 2*B*).

Lipid Metabolism in CerS1$^{-/-}$ Mice—Ceramide synthase activity was determined in the brains of 6-week-old wild type and CerS1$^{-/-}$ mice. The CerS1$^{-/-}$ mice showed a reduction in ceramide synthase activity toward C18 acyl-CoAs by 78% relative to wild type controls (data not shown). The results confirm a substrate specificity of CerS1 for C18:0 acyl chain (15–17). Zhao *et al.* (17) reported lipid analyses only from brains of 2-week-old mice. In addition, we determined the levels of free long chain base, long chain base phosphates, ceramides, hexosylceramides, sphingomyelin, sulfatides, and gangliosides in lipid extracts of cerebellum and forebrain of 6-week- and 18-month-old CerS1$^{+/+}$ and CerS1$^{-/-}$ mice (Fig. 3). Nanoelectrospray ionization-tandem mass spectrometry revealed that the amounts of neutral d18:1-C18 sphingolipids (ceramide (Fig. 3*A*), hexosylceramide (Fig. 3*B*), and sphingomyelin (Fig. 3*C*)) in forebrain and cerebellum were reduced. The amounts of d20:1-containing neutral sphingolipids were very low. The quantification of GD1 and SM4 was based on the characteristic fragment obtained from sialic acid and sulfate, respectively. Because of this, isobaric acidic sphingolipids like d18:1,C20:0 and d20:1,C18:0 cannot be distinguished and are therefore presented as the sum of carbon atoms:number of double bonds. The amounts of Σd36:1 representing sphingolipids containing d18:1,C18:0 and Σd38:1 (d18:1,C20:0 and d20:1,C18:0) in forebrain and cerebellum were reduced.

In 6-week-old mice, the total amounts of ceramide, hexosylceramide (supplemental Fig. S2), sphingomyelin, and sulfatide (supplemental Fig. S3) were not changed due to an increase of other molecular species with different chain lengths, suggesting compensation by other ceramide synthases. However, the total amount of GD1 was decreased to 50% in forebrain and cerebellum of CerS1$^{-/-}$ mice compared with control mice (Fig. 4, *A* and *D*).

In 18-month-old mice, we observed not only a decrease of C18 sphingomyelin and C18 hexosylceramide but also a decrease of all other sphingomyelin (Fig. 3*C*) and hexosylceramide (Fig. 3*B*) molecular species, leading to a decrease of the total amount of hexosylceramides to 40% and a decrease of the total amount of sphingomyelin to 50%. In these 18-month-old mice, the levels of sphinganine and sphingosine, both substrates of ceramide synthases, were increased in the cerebellum by 2- and 4-fold, respectively, and to a much lesser extent in the forebrain (Fig. 3*D*). Sphingosine 1-phosphate and sphinganine 1-phosphate were also increased in cerebella and forebrains of 18-month-old CerS1$^{-/-}$ mice (supplemental Fig. S4) probably due to increased levels of the substrates of LCB kinase, sphingosine and sphinganine, respectively.

Gangliosides in forebrain and cerebellum of 18-month-old mice were analyzed by thin layer chromatography (Fig. 4, *B* and *E*). The levels of all major brain ganglioside classes were decreased in CerS1$^{-/-}$ relative to wild type mice. In CerS1$^{-/-}$ cerebellum, GD1a was decreased to 30%, GM1 was decreased to 36%, GT1b showed a reduction to 56%, and GD1b showed a reduction to 19% (Fig. 4*C*). Also in forebrain, we measured a decrease in the major ganglioside classes (GM1, 55%; GD1a, 72%; GT1b, 37%; GD1b, 59%) (Fig. 4*F*). As GD1 and GT1b are known to serve as complementary ligands for MAG (13, 14), we investigated the expression level of MAG in CerS1$^{-/-}$ and CerS1$^{+/+}$ mice (Fig. 4*G*). We found that MAG was down-regulated by 60% in cerebellum and forebrain (Fig. 4*H*). To determine whether only MAG protein or also the total myelin was decreased in CerS1$^{-/-}$ mice, we investigated the expression

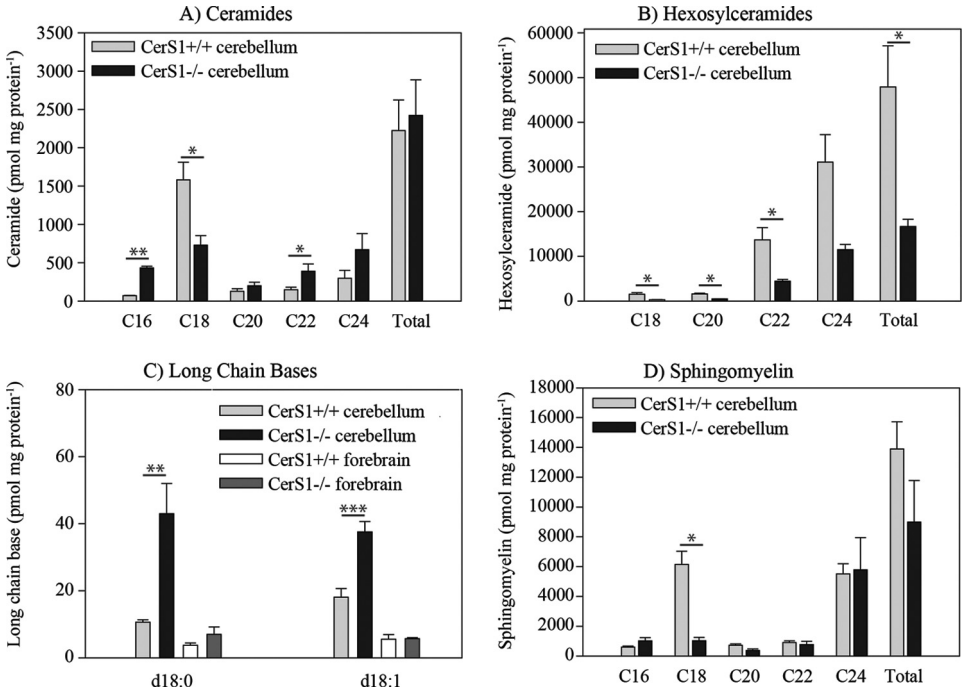

FIGURE 3. **Quantitative lipid analyses of neutral sphingolipids in CerS1$^{-/-}$ mice in comparison with wild type mice.** A quantitative evaluation of ceramide (*A*), hexosylceramide (*B*), sphingomyelin (*C*), and long chain bases (*D*) in the cerebellum of 18-month-old mice ($n = 3$) by nanoelectrospray ionization-MS/MS is shown. The lipid content measured in three animals (mean and S.E. (*error bars*)) is shown. Lipids are classified by their acyl chain length. The decrease of different sphingolipids with C18 acyl chain length in CerS1$^{-/-}$ mice relative to wild type mice is obvious in all cases. There is an increase of ceramides containing acyl groups with other chain lengths, leading to a balanced amount of total ceramide. In contrast, there is no such balancing effect in the hexosylceramide class or in the sphingomyelin class by sphingolipids with other acyl chain lengths. *Stars* indicate statistically significant difference, when compared with wild type controls (*, $p < 0.05$; **, $p < 0.01$; ***, $p < 0.001$; *t* test).

level of myelin basic protein (MBP) in CerS1$^{-/-}$ and CerS1$^{+/+}$ mice (Fig. 4*I*) and found it to be about the same.

Histological Abnormalities of CerS1$^{-/-}$ Mice—Within the CNS of CerS1-deficient mice, morphological abnormalities were mainly observed in the cerebellum, affecting its size and macroscopic organization as well as the survival of its major neurons. The normal cerebellum is made up of an elaborate set of folia separated by fissures (40). Already during postnatal development of the CerS1$^{-/-}$ mice, we noticed a discrete foliation defect, *i.e.* the absence of a fissure separating folia VI and VII. In contrast, cerebellar lamination developed correctly without major ectopia and within a normal time frame (Fig. 5, *E* and *F*). Macroscopically, we observed a mainly postdevelopmental size reduction, first affecting the vermis (43% less weight in 6-week-old mice), but between 6 and 12 months postnatally also causing a significant atrophy of cerebellar hemispheres (Fig. 5, *A–D*).

Likewise, occurring mainly after completion of cell positioning around postnatal day 20, initially normal appearing Purkinje neurons started to degenerate throughout all folia with the majority of these cells disappearing until the 6th month postnatally (Fig. 5, *G* and *H*), confirming results by Zhao *et al.* (17). Less conspicuously, postmigratory granule cells (*i.e.* within the internal granular layer) also showed a 6 times increased rate of apoptosis as early as postnatal day 10 as tested with TUNEL assays (Fig. 5*J*) and visualized by microscopic appearance (Fig. 5*I*). Interestingly, significant astrogliosis was only observed in the cerebellar white matter but was absent from its neuronal strata (Fig. 5, *K* and *L*). Likewise, activation of microglia as measured by RCA1 binding was absent from all brain regions.

Zhao *et al.* (17) described accumulation of lipofuscin in many regions of the brain. In our CerS1$^{-/-}$ mice, minor accumulation of a brown pigment was only found in sensory ganglion cells of the peripheral nervous system, especially in the trigeminal ganglion (data not shown).

Open Field Exploration, Habituation, and Dishabituation—Deficiency in different ganglioside synthases causes various behavioral phenotypes in mice including motor and neuropsychological impairment (41–43). We found a behavioral impairment in our CerS1$^{-/-}$ mice that increased with age. We performed different tests to evaluate the motor function and learning abilities of CerS1$^{-/-}$ mice. CerS1$^{-/-}$ and CerS1$^{+/+}$ mice showed reduced locomotion across the three habituation trials in the open field (main effect of trials: CerS1$^{-/-}$, $F(2,14) = 15.67$, $p < 0.001$; CerS1$^{+/+}$, $F(2,12) = 8.78$, $p = 0.004$; repeated measures analysis of variance; Fig. 6*A*). Furthermore, both groups exhibited reductions in the mean running speed (CerS1$^{-/-}$, $p < 0.001$; CerS1$^{+/+}$, $p < 0.01$; Fig. 6*B*). There was no significant genotype × trial interaction for the measures locomotion and mean running speed ($p > 0.05$), suggesting that behavioral habituation to the open field was not affected in the CerS1$^{-/-}$ mice. However, CerS1$^{-/-}$ mice exhibited significantly decreased locomotion over the three trials in the open field (main effect of genotype: $F(1,13) = 177.76$, $p = 0.003$; Fig. 6*A*). CerS1$^{-/-}$ mice also showed significantly decreased mean running speed across the three trials (main effect of genotype: $F(1,13) = 177.71$, $p = 0.003$; Fig. 6*B*). Hence, these data indicate

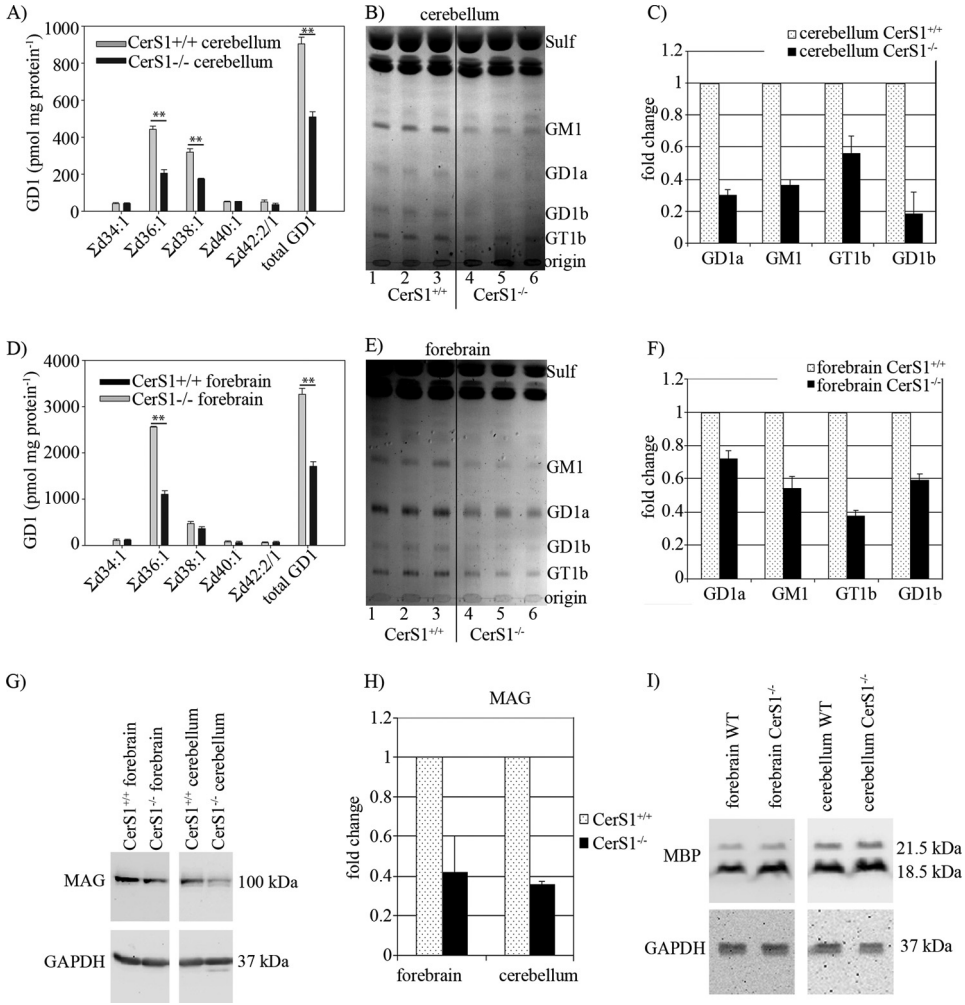

FIGURE 4. **Accumulation of gangliosides of forebrain and cerebellum and immunoblot of myelin-associated glycoprotein.** A quantitative evaluation of GD1 in the cerebellum (*A*) and forebrain (*D*) of 6-week-old mice is shown. Doubly charged ions were recorded in nanoelectrospray ionization-MS/MS. Lipids are classified by their total number of carbon atoms:number of double bonds of the ceramide moiety. The lipid content measured in three animals is displayed. The lipid content measured in three animals (mean and S.E. (*error bars*)) is shown. *B* and *E*, lipid analyses of cerebellum and forebrain of 18-month-old mice by TLC. Lipids were applied according to equal amounts of protein. Positions of lipid standards are indicated. *Sulf*, sulfatide. *C* and *F*, quantification of TLC analyses of gangliosides. The lipid content measured in three animals (mean and S.D. (*error bars*)) is shown. *G*, immunoblot analysis of MAG from forebrain and cerebellum extracts of 6-week-old CerS1$^{+/+}$ and CerS1$^{-/-}$ mice. In addition, blots were performed with anti-GAPDH to control equal loading of the gels. *H*, quantification of MAG protein in 6-week-old CerS1$^{-/-}$ mice in comparison with CerS$^{+/+}$ mice. In CerS1$^{-/-}$ mice, MAG is decreased by about 60% ($n = 3$). The MAG content measured in three animals (mean and S.E. (*error bars*)) is shown. *I*, immunoblot analysis of myelin basic protein (*MBP*) in forebrain and cerebellar extracts of 6-week-old CerS1$^{+/+}$ and CerS1$^{-/-}$ mice ($n = 3$). GAPDH serves as a loading control. *Stars* indicate statistically significant difference, when compared with wild type controls (**, $p < 0.01$; *t* test).

that CerS1$^{-/-}$ mice exhibit a decrease in locomotor activity and running speed in the open field, suggesting that CerS1 deficiency impairs motor function. The dishabituation indices of the fourth trial of open field testing were not significantly different between CerS1$^{-/-}$ and CerS1$^{+/+}$ mice ($p < 0.05$, Student's *t* test for independent groups; not shown).

Across the three habituation trials, the time spent in the corners increased (main effect of trials: CerS1$^{+/+}$, $F(2,14) = 9.76$, $p = 0.002$; Fig. 6*C*), whereas the time spent in the center decreased (main effect of trials: $F(2,14) = 8.74$, $p = 0.003$; Fig. 6*D*) in the CerS1$^{+/+}$ group. In contrast, neither the time spent in the corners ($p > 0.05$) nor the time spent in the center ($p = 0.52$) changed significantly across the three trials in the CerS1$^{-/-}$ group. Compared with CerS1$^{+/+}$, the CerS1$^{-/-}$ mice spent significantly less time in the corners (main effect of genotype: $F(1,13) = 13.68$, $p = 0.003$; Fig. 6*C*) and more time in the center (main effect of genotype: $F(1,13) = 8.20$, $p = 0.01$; Fig. 6*D*). These results suggest a possible anxiolytic effect in CerS1$^{-/-}$ mice. However, this behavioral pattern might also be explained by a prolonged period of immobility of the CerS1$^{-/-}$ mice after their placement into the center of the open field. No significant genotype × trials interactions were found for the time spent in the corners ($F(2,26) = 0.121$, $p = 0.88$) and center time ($p > 0.05$) variables.

The CerS1$^{-/-}$ mice also exhibited reduced running speed in the center relative to the CerS1$^{+/+}$ mice (main effect of genotype: $F(1,13) = 29.073$, $p < 0.001$; Fig. 6*E*). No significant genotype × trial interaction was found for the mean running speed in the center variable ($p > 0.05$).

Motor Coordination Learning and Long Term Memory—The rotarod performance of both CerS1$^{-/-}$ (main effect of trials: CerS1$^{-/-}$, $F(8.56) = 4.552$, $p = 0.0001$; Fig. 6*F*) and CerS1$^{+/+}$

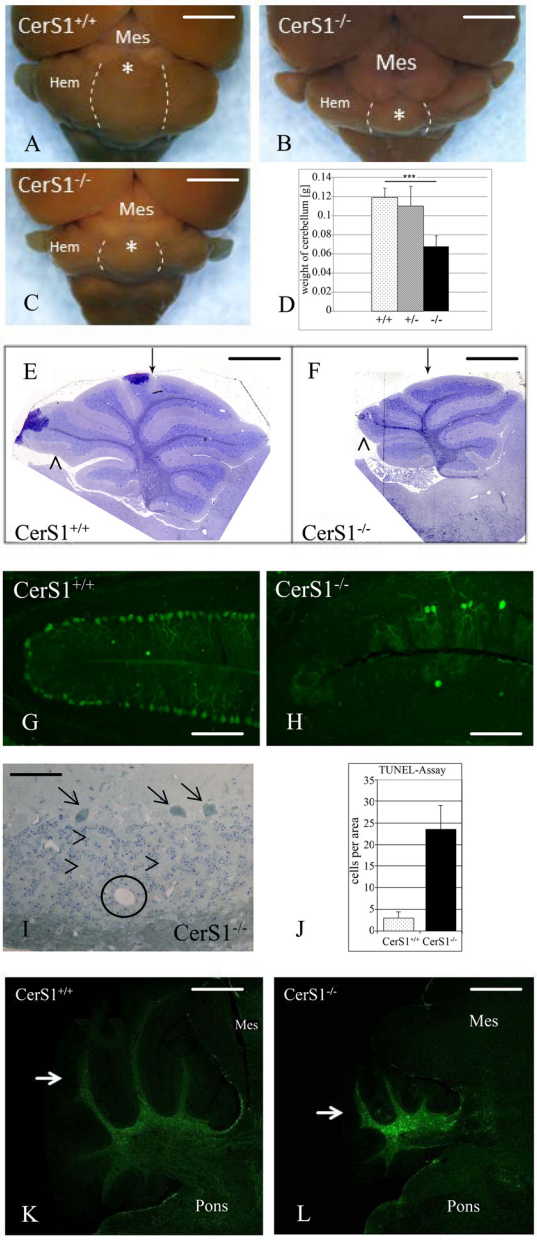

FIGURE 5. **CerS1 deficiency causes foliation defects and postnatal neurodegeneration in the cerebellum.** *A–C*, cerebellum and brain stem (dorsal aspect) as seen in an adult wild type mouse (*A*) and CerS1$^{-/-}$ mice of 2 months (*B*) and 12 months (*C*) of age. Note the progressive shrinkage of the cerebellum, first evident by the retraction of the anterior vermis (*asterisk*) from the caudal colliculi already at 2 months. Shrinkage of cerebellar hemispheres (*Hem*) starts more slowly and is most pronounced during the second half of the 1st year postnatally. *Dotted lines* indicate the border between the vermis and hemispheres. Note that the flocculonodular lobe almost retains its normal size. At 12 months, the cerebellum is reduced to a flat band covering the dorsal pons. However, the relative loss of volume still appears greatest in the vermal region. Quantitatively, the postnatal cerebellum from 6-week-old mice loses about 50% of its normal weight (*D*). Interestingly, a limited weight loss is seen in heterozygous mice. *Bars* represent mean + S.E. (*error bars*) of weight of cerebellum. *Stars* indicate statistically significant difference, when compared with wild type controls (***, $p < 0.001$; *t* test). *E* and *F*, CerS1-deficient mice feature a modified cerebellar foliation pattern already during postnatal development characterized by the absence of a short fissure separating lobules VI and VII (*arrow*) and less consistently by the absence of a short fissure splitting the apical part of lobule IX (*arrowhead*). *G–J*, neurodegeneration affects both Purkinje neurons (*G* and *H*) and granule cells (*I* and *J*). Loss of Purkinje cells, visualized here by anti-calbindin staining in *G* and *H* and marked by *arrows* in *I*, mainly starts after completion of lamina formation around postnatal day 20 and leads to a subtotal loss of these cells by the end of the first year. Due to their extremely high number, loss of granule cells is on first glance less impressive in routine preparations of early adult cerebella, mainly identified by small cysts filled with debris (*circle* in *I*) and an unusually wide scattering of cells in an internal granular layer now more dominated by interstitial territories of mossy fiber boutons (*arrowheads* in *I*). However, a strongly increased extent of granule cell apoptosis is already present in postmigratory cells of the anterior lobe (*J*), the first cerebellar region showing shrinkage. *Bars* represent mean + S.E. (*error bars*) of apoptotic cells per area. *K* and *L*, in contrast to the mainly neuronal damage, astrogliosis is most prominent in the cerebellar white matter but surprisingly less so in neuronal strata. However, this finding again shows that changes in the axonal sphingolipid profile might have an impact on different cell types. *Mes*, *mesencephalon*. *Calibration bars*, 2 mm in *A*, *B*, and *C*, 1 mm in *E* and *F*, 150 μm in *G* and *H*, 50 μm in *I*, and 750 μm in *K* and *L*.

mice (CerS1$^{+/+}$, $F(8.48) = 5.827$, $p = 0.0001$) improved significantly across the nine acquisition trials. Acquisition was significantly impaired in CerS1$^{-/-}$ as compared with CerS1$^{+/+}$ mice (main effect of genotype: CerS1$^{-/-}$ *versus* CerS1$^{+/+}$, $F(1.13) = 9.679$, $p = 0.008$; Fig. 6*F*). However, no significant genotype × trial interaction was evident ($p > 0.05$). A retest performed 2 weeks after the last acquisition trial confirmed the impaired performance of CerS1$^{-/-}$ as compared with the CerS1$^{+/+}$ mice ($p < 0.05$).

Vertical Pole Test—No significant difference between CerS1$^{-/-}$ and CerS1$^{+/+}$ mice (p values >0.05, Mann-Whitney *U* test; supplemental Table S1) regarding the time needed to perform the 180° turn was found. The total time needed to climb down the pole on trial 2 was significantly increased in the CerS1$^{-/-}$ mice ($p = 0.01$; supplemental Table S1). No significant genotype difference was observed on trial 1 ($p > 0.05$). The CerS1$^{+/+}$ mice needed significantly less time to climb down the pole on the second as compared with the first trial ($p = 0.01$, Wilcoxon test), whereas CerS1$^{-/-}$ mice performed similarly on both trials ($p > 0.05$). The latter result suggests impaired motor learning in CerS1$^{-/-}$ mice.

Horizontal Wire Test—On trial 1, the duration of active performance was significantly higher in CerS1$^{+/+}$ as compared with CerS1$^{-/-}$ mice ($p = 0.01$, Mann-Whitney *U* test; supplemental Table S1). However, this difference was no longer present during trial 2 ($p > 0.05$). On trial 2, CerS1$^{+/+}$ mice performed superiorly to the CerS1$^{-/-}$ mice ($p = 0.02$), suggesting an impairment in neuromotor functions in CerS1$^{-/-}$ mice. No change in the dependent measures was evident between the first and the second trial either in CerS1$^{+/+}$ or CerS1$^{-/-}$ mice (p values >0.05, Wilcoxon test).

Spontaneous Alternation Performance in the Y-maze—The CerS1$^{-/-}$ mice showed a reduced number of triplets ($T = 3.16$, $df = 13$, $p = 0.007$; Fig. 6*G*) and total arm entries ($p = 0.01$) as compared with the CerS1$^{+/+}$ mice. To assess spatial working memory of the CerS1$^{-/-}$ mice independently of motor activity, we calculated an alternation index that is not dependent on the number of arm entries. CerS1$^{+/+}$ mice exhibited significantly higher alternation ratios relative to the CerS1$^{-/-}$ mice ($T = 2.42$, $df = 13$, $p = 0.03$, Student's *t* test for non-paired data; Fig. 6*G*). The alternation index of CerS1$^{+/+}$ mice was higher than the chance level ($T = 3.42$, $df = 7$, $p = 0.01$, single group *t* test), whereas that of the CerS1$^{-/-}$ mice was not different from the chance level ($p = 0.526$), suggesting that CerS1 deficiency leads to impairments in spatial working memory.

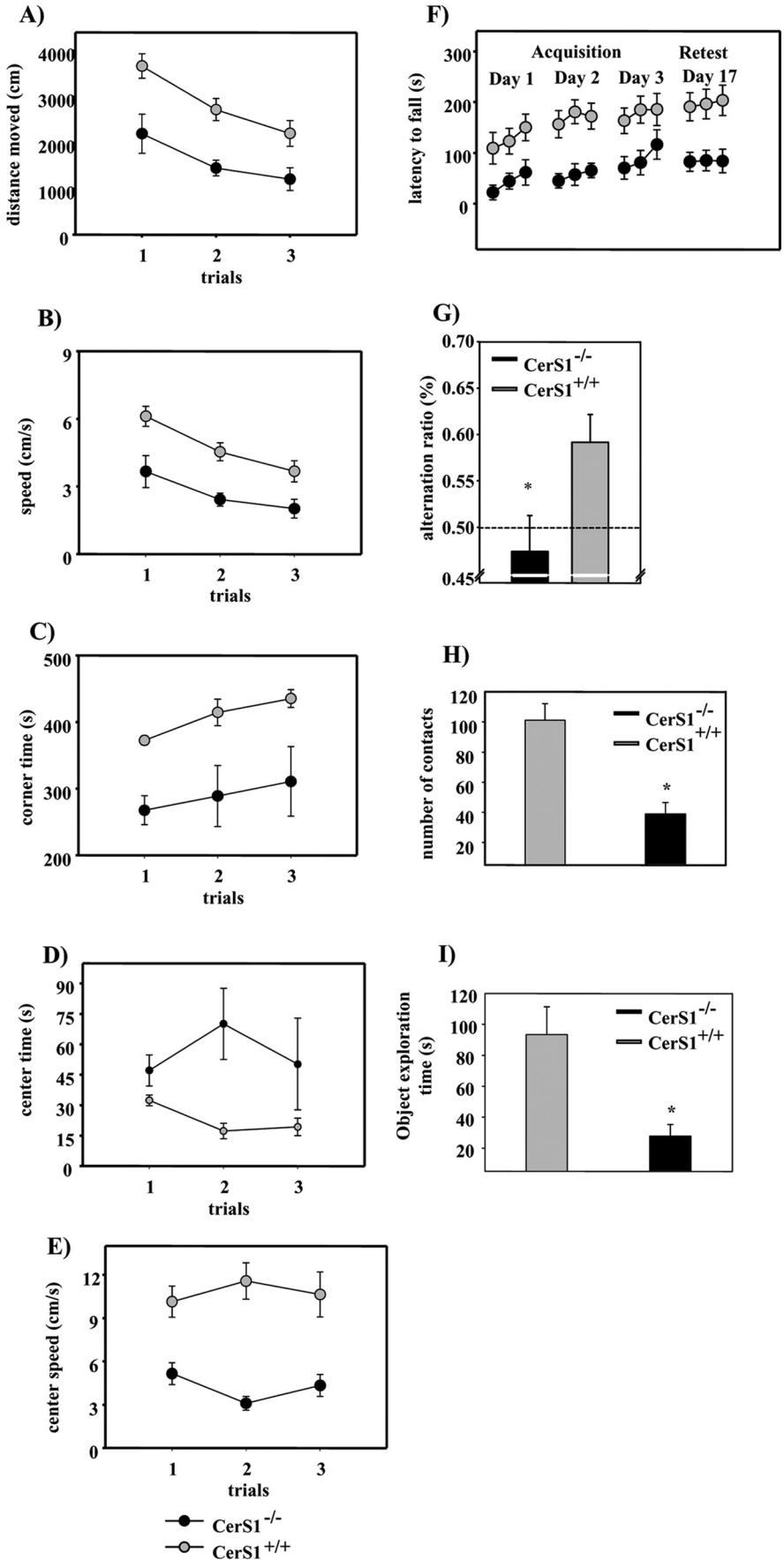
A)
distance moved (cm)
4000
3000
2000
1000
0
1
2
3
trials
B)
speed (cm/s)
9
6
3
0
1
2
3
trials
C)
corner time (s)
500
400
300
200
1
2
3
trials
D)
center time (s)
90
75
60
45
30
15
0
1
2
3
trials
E)
center speed (cm/s)
12
9
6
3
0
1
2
3
trials
CerS1 -/-
CerS1 +/+
F)
Acquisition
Retest
Day 1
Day 2
Day 3
Day 17
latency to fall (s)
300
200
100
0
G)
alternation ratio (%)
0.70
0.65
0.60
0.55
0.50
0.45
*
CerS1 -/-
CerS1 +/+
H)
number of contacts
120
100
80
60
40
20
*
CerS1 -/-
CerS1 +/+
I)
Object exploration time (s)
120
100
80
60
40
20
*
CerS1 -/-
CerS1 +/+

Novel Object Exploration Test—The CerS1$^{+/+}$ mice showed a significantly higher number of object contacts (CerS1$^{+/+}$, 101.13 ± 11.11; CerS1$^{-/-}$, 38.86 ± 7.64; $T = 4.48$, $df = 13$, $p = 0.001$, Student's t test for unpaired data; Fig. 6*H*) and object exploration time (CerS1$^{+/+}$, 93.37 ± 17.95; CerS1$^{-/-}$, 27.74 ± 7.50; $p = 0.007$; Fig. 6*I*) as compared with CerS1$^{-/-}$ mice. Furthermore, the CerS1$^{+/+}$ mice exhibited significantly higher levels of locomotion relative to CerS1$^{-/-}$ mice ($p < 0.001$, Student's t test for unpaired data; not shown). Our data suggest that CerS1$^{-/-}$ mice are probably less motivated to approach and explore novel objects as compared with the CerS1$^{+/+}$ mice. Again, it remains to be determined how much of this effect is due to motor impairments, *e.g.* the inability to rear or lean on the object.

DISCUSSION

CerS1$^{-/-}$ mice were generated by homologous recombination in embryonic stem cells. In these mice, parts of the catalytic domain of CerS1 were deleted and replaced by the *egfp* gene, which should be expressed as a fusion protein together with the C-terminal peptide of CerS1. However, the expected fusion protein was not found by eGFP fluorescence or staining with anti-GFP. The transcript of the mutated gene could easily be observed with probes against *gfp* or *cers1* in Northern blot analyses. Thus, we generated polyclonal antibodies to the C terminus of CerS1 because at this time several commercially available antibodies yielded unspecific signals in CerS1-deficient tissue. Using the new custom-made antibodies, we found the CerS1 protein in brain of wild type mice but not in that of CerS1-deficient mice. We conclude that the fusion protein is not translated as mRNA appears to be present or rapidly degraded in CerS1-deficient brain. The predicted molecular mass of CerS1 protein is 37 kDa. The smaller mass of the detected protein could be due to altered detergent binding of membrane proteins (44).

The results of ceramide synthase assays with brain homogenates of CerS1$^{-/-}$ mice were consistent with the absence of CerS1 activity because ceramide synthase activity toward C18 fatty acyl-CoA was significantly decreased by 78% in extracts of CerS1$^{-/-}$ brain. The remaining synthesis capacity for C18 ceramide is likely due to the activity of other CerS proteins in the brain.

With the new CerS1-specific antibodies, we determined by immunofluorescence analyses that the CerS1 protein is exclusively expressed in neurons. This result confirms earlier data obtained by *in situ* hybridization of *cers1* mRNA (45).

Mass spectrometric analyses of ceramides in forebrain and cerebellum of CerS1$^{-/-}$ mice also confirmed *in vitro* data (15, 16) on fatty acid specificity of CerS1. In the previous study of Zhao *et al.* (17), the lipid levels of 2-week-old mice were examined. At this age, the development of the brain is not yet complete. Thus, we investigated later stages of development. The analysis of lipids in 6-week-old mice showed the same relative differences between wild type and CerS1$^{-/-}$ mice as observed in 2-week-old mice for ceramide, sphingomyelin, and hexosylceramide. In addition, we found a decrease of sphingolipids with C18 acyl chain length in CerS1$^{-/-}$ mice relative to wild type mice in all sphingolipid classes. The levels of sphingolipids containing other acyl chains, i.e. C16, C20, C22, and C24:1, were increased, leading to a balanced amount of total sphingolipids between CerS1$^{-/-}$ and wild type brains. These results are in line with data from CerS2 knock-out mice in which compensation effects were also observed (25, 46). Recent cell culture experiments showed that CerS proteins build dimers and increase activity by dimerization (47). However, cell type-specific expression patterns of CerS proteins in the brain and additional mechanisms of regulation at the transcriptional and posttranscriptional levels might add to the regulation of CerS activities *in vivo*.

Different results were obtained for 18-month-old CerS1 KO mice. We found that sphingomyelin and hexosylceramides with C18 acyl chains but unexpectedly also lipids with other acyl chains were decreased, leading to a decreased level of total sphingolipid classes. It seems that the balancing effect is not maintained during the life span of a mouse.

In agreement with data from young mice, we also noticed that the amounts of sphingosine and sphinganine were increased in 18-month-old mice. As the accumulation of sphingosine has been shown to result in cell death (48, 49), one could hypothesize that increased sphingosine levels may lead to neurodegeneration of Purkinje cells.

The major brain ganglioside classes (GM1, GD1a, GD1b, and GT1b) were significantly decreased in the CerS1$^{-/-}$ brain in comparison with wild type brain. When we checked the fatty acyl chains in the gangliosides, we found that C18 GD1 (Σd36:1 and Σd38:1) was decreased and that there was no change in the other chain lengths, leading to a decrease in the total amount of gangliosides. This leads to the assumption that gangliosides in the brain originate mostly from CerS1-derived ceramide.

Several mutant mouse lines were reported in which different enzymes responsible for ganglioside synthesis were altered or depleted (11). The phenotypes of these mice ranged from subtle to severe abnormalities. For example, mice lacking *N*-acetylgalactosaminyltransferase and as a consequence GalNAc-containing gangliosides (including GD1a and GT1b) exhibit neurological disorders such as axonal degeneration; sensory, motor, and behavior insufficiencies; and other neural dysfunc-

FIGURE 6. **Behavioral phenotyping of CerS1$^{-/-}$ mice.** *A*, locomotion in the open field. *Circles* represent mean ± S.E. (*error bars*) locomotion (distance moved in cm) on the indicated trials. *B*, running speed. *Circles* represent mean ± S.E. (*error bars*) running speed (cm/s) on the indicated trials in the open field. *C*, corner time. *Circles* represent mean ± S.E. (*error bars*) time spent (s) in the corner zones of the open field on the indicated trials. *D*, center time. *Circles* represent mean ± S.E. (*error bars*) time spent (s) in the center zone of the open field on the indicated trials. *E*, center speed. *Circles* represent mean ± S.E. (*error bars*) running speed (cm/s) on the indicated trials in the center zone of the open field. *F*, motor coordination and balancing performance. *Circles* represent mean ± S.E. (*error bars*) latency to fall (s) from the accelerating rotarod on the indicated days of acquisition and the retest day. *G*, spatial alternation behavior in the Y-maze. *Bars* represent mean ± S.E. (*error bars*) alternation ratios. *, $p < 0.05$, Student's t test for non-paired data. The *dashed line* indicates performance at the chance level. *H*, contacts with a novel object. *Bars* represent mean ± S.E. (*error bars*) number of contacts in the novel object exploration test. *, $p < 0.05$, Student's t test for non-paired data. *I*, novel object exploration time. *Bars* represent mean ± S.E. (*error bars*) time spent exploring the novel objects. *, $p < 0.05$, Student's t test for non-paired data.

tions (41). It has been shown that complex gangliosides are involved in neural development and maintenance of neural functions. Gangliosides are primarily localized in the outer leaflets of plasma membranes of neurons and are known to function in cell-cell recognition and signal transduction (11). MAG is expressed on the innermost myelin sheet directly apposed to the axon surface and has been shown to bind to gangliosides GD1a and GT1b located on the neuronal membrane (14). In our study, we found that MAG expression decreased by 60% in the CerS1$^{-/-}$ mice, indicating an effect of neuron-specific gangliosides on a protein expressed solely in oligodendrocytes. There appears to be no change in the myelin sheaths because the level of myelin basic protein was very similar in wild type and homozygous CerS1$^{-/-}$ mice. A similar effect has been noticed before, but its origin was different: mice deficient for *N*-acetylgalactosaminyltransferase show an age-dependent decrease in MAG protein (50). MAG mRNA levels in these mice were unaffected, indicating decreased stability of the MAG protein in the absence of its ganglioside ligands. The similar reduced level of MAG in the CerS1$^{-/-}$ mice where gangliosides were reduced by only 60% suggests a threshold of ganglioside concentration necessary for MAG stabilization. Alternatively, the distribution of gangliosides (in axons, cell body, or synapses) might be altered in CerS1 KO mice, and ganglioside levels in the axonal membrane might be much more strongly decreased than in other membranes of the neuron. The described phenotype of CerS1$^{-/-}$ mice is unlikely to be only subsequent to reduction in MAG expression because this reduction is not complete (60%), and mice heterozygous for the MAG allele were reported to have similarly reduced MAG expression, but they lack any of the described phenotypes (51).

Mice deficient for MAG protein exhibit neural degeneration and behavioral abnormalities similar to *N*-acetylgalactosaminyltransferase-deficient mice (14). In our behavioral tests, CerS1$^{-/-}$ mice showed significantly decreased locomotion and running speed in the open field. In addition, we found an anxiolytic behavioral profile with significantly increased time spent in the center and decreased time spent in the corners of the open filed. The Y-maze alternation performance was impaired, and performance in the rotarod assay and novel object exploration were compromised. MAG- and *N*-acetylgalactosaminyltransferase-deficient mice also show impaired motor balance, coordination, and muscle control, but despite motor behavioral deficits, these mutant mouse strains were hyperactive with total spontaneous locomotor activity increased 60–130% above that of wild type mice (14), which stands in contrast to the results for our CerS1-deficient mouse line.

Currently available data on the function of sphingolipids and derived gangliosides in the cerebellum also fit well with the observed neurodegeneration. For instance, the generalized abrogation of the synthesis of complex sphingolipid compounds by a selective knock-out of glucosylceramide synthase in Purkinje cells (52) causes progressive loss of these cells from adult cerebella within the same time frame as seen in our mice, but it is less severe in terms of numerical cell loss. Among other functions, gangliosides play a major role in the stabilization and function of glycolipid-rich membrane microdomains, and interference with their synthesis by ablation of specific glycosyltransferases likewise resulted in adult onset neurodegeneration (53). However, we did not observe obvious defects in dendritic arborization *in vivo* that have been noted in *in vitro* assays in glycosphingolipid-deficient mice.

Although neurodegeneration and subsequent cerebellar shrinkage are in good accordance with published data on glycosphingolipid function in cerebellum, the pathogenesis of the limited foliation defect seen in our mice is less clear, the more so as a wide variety of (unrelated) genetic defects both in mice and man result in similar alterations. For instance, related phenotypes have been reported from Zic4-deficient mice, interpreted as a murine form of a Dandy-Walker malformation (54). In these mice, foliation defects are attributed to impaired granule cell proliferation. Although we observed granule cell loss mainly in the anterior cerebellum during development, it was not focused to folia VI/VII. A similar localized foliation defect but in this case associated with subpial ectopia of granule cells that failed to migrate from their proliferative matrix toward the inner granular layer has been reported with ether lipid-deficient mice (55). In this case, defective lipid raft domains causing subsequent defects of multiple signaling pathways were proposed to be involved in the pathogenesis, which could result in pathomechanisms similar to those envisaged for CerS1 deficiency in which gangliosides enriched in rafts are not synthesized at normal levels. Interestingly, the authors discuss focally disturbed proliferation of granule cells in the external granular layer, which could fit to the inconstantly observed thinning of the external granular layer in the anterior lobus posterior in our material. However, a virtually identical localized foliation defect has been reported after knock-out of the nuclear orphan receptor and putative transcription regulator tak1 (56) and was hypothetically related to maldifferentiation, but not cell death, of Purkinje neurons during development.

Our study demonstrates that the lipid changes and reduced expression of MAG are not limited to the cerebellum of CerS1$^{-/-}$ mice but also involve the forebrain of CerS1$^{-/-}$ mice. The changes in the CerS1$^{-/-}$ mice are not only found in neurons of the brain but also affect neighboring oligodendrocytes. Our results reveal that MAG expression in oligodendrocytes is dependent on CerS1-derived neuronal gangliosides in cerebellum and in forebrain. Furthermore, C18 ceramide is required as a precursor for the biosynthesis of gangliosides in cerebellum and forebrain. It remains to be clarified which enzymes involved in ganglioside biosynthesis are restricted to C18 lipid precursor molecules.

The CerS1-deficient mice are a useful model to study the effects of decreased but not absent ganglioside levels in mice. In humans, it has been shown that varying ganglioside levels can be responsible for different neuropathological diseases. Several years ago, a study showed that a homozygous loss-of-function mutation of GM3 causes infantile onset symptomatic epilepsy syndrome (57). For Huntington disease patients, it has very recently been shown that synthesis of ganglioside GM1 is reduced (observed in fibroblast from patients and in cell and animal models of Huntington disease). Furthermore, it has been found that decreased GM1 levels contribute to increased Huntington disease cell susceptibility to apoptosis (58).

Recently, it was reported that sphingomyelin with C18:0 fatty acyl residue binds to p24 protein of COPI vesicles involved in intracellular protein trafficking (59). These analyses have been carried out with cultured HeLa cells and Chinese hamster ovary (CHO) cells. It remains to be investigated whether or not CerS1 deficiency influences intracellular protein trafficking via COPI vesicles. With our study, we have started to unravel the functions of CerS1-derived lipids and their interaction partners, and we hypothesize that the behavioral phenotype of CerS1$^{-/-}$ mice may not only be determined by alteration in one lipid class but by several changes in lipid levels and related interacting proteins in the whole brain.

Acknowledgments—We thank L. Manns, C. Siegmund, M. Jokwitz, B. Rau, and A. Zoons (University of Bonn) for technical assistance and Prof. Dr. M. Egmond (University of Utrecht) for providing the immunogenic CerS1 peptide.

REFERENCES

1. Liu, B., Obeid, L. M., and Hannun, Y. A. (1997) Sphingomyelinases in cell regulation. *Semin. Cell Dev. Biol.* **8,** 311–322
2. Ogretmen, B., and Hannun, Y. A. (2001) Updates on functions of ceramide in chemotherapy-induced cell death and in multidrug resistance. *Drug Resist. Updat.* **4,** 368–377
3. Mullen, T. D., Hannun, Y. A., and Obeid, L. M. (2012) Ceramide synthases at the centre of sphingolipid metabolism and biology. *Biochem. J.* **441,** 789–802
4. Kolter, T., and Sandhoff, K. (1999) Sphingolipids—their metabolic pathways and the pathobiochemistry of neurodegenerative diseases. *Angew. Chem. Int. Ed. Engl.* **38,** 1532–1568
5. Mencarelli, C., and Martinez-Martinez, P. (2012) Ceramide function in the brain: when a slight tilt is enough. *Cell. Mol. Life Sci.*, in press
6. Sandhoff, R. (2010) Very long chain sphingolipids: tissue expression, function and synthesis. *FEBS Lett.* **584,** 1907–1913
7. Merrill, A. H., Jr. (2002) *De novo* sphingolipid biosynthesis: a necessary, but dangerous, pathway. *J. Biol. Chem.* **277,** 25843–25846
8. Wang, B., Shi, G., Fu, Y., and Xu, X. (2007) Cloning and characterization of a LASS1-GDF1 transcript in rat cerebral cortex: conservation of a bicistronic structure. *DNA Seq.* **18,** 92–103
9. Spassieva, S., Seo, J. G., Jiang, J. C., Bielawski, J., Alvarez-Vasquez, F., Jazwinski, S. M., Hannun, Y. A., and Obeid, L. M. (2006) Necessary role for the Lag1p motif in (dihydro)ceramide synthase activity. *J. Biol. Chem.* **281,** 33931–33938
10. Kolter, T., Proia, R. L., and Sandhoff, K. (2002) Combinatorial ganglioside biosynthesis. *J. Biol. Chem.* **277,** 25859–25862
11. Yu, R. K., Tsai, Y. T., and Ariga, T. (2012) Functional roles of gangliosides in neurodevelopment: an overview of recent advances. *Neurochem. Res.* **37,** 1230–1244
12. van Echten-Deckert, G., and Walter, J. (2012) Sphingolipids: critical players in Alzheimer's disease. *Prog. Lipid Res.* **51,** 378–393
13. Yang, L. J., Zeller, C. B., Shaper, N. L., Kiso, M., Hasegawa, A., Shapiro, R. E., and Schnaar, R. L. (1996) Gangliosides are neuronal ligands for myelin-associated glycoprotein. *Proc. Natl. Acad. Sci. U.S.A.* **93,** 814–818
14. Pan, B., Fromholt, S. E., Hess, E. J., Crawford, T. O., Griffin, J. W., Sheikh, K. A., and Schnaar, R. L. (2005) Myelin-associated glycoprotein and complementary axonal ligands, gangliosides, mediate axon stability in the CNS and PNS: neuropathology and behavioral deficits in single- and double-null mice. *Exp. Neurol.* **195,** 208–217
15. Laviad, E. L., Albee, L., Pankova-Kholmyansky, I., Epstein, S., Park, H., Merrill, A. H., Jr., and Futerman, A. H. (2008) Characterization of ceramide synthase 2: tissue distribution, substrate specificity, and inhibition by sphingosine 1-phosphate. *J. Biol. Chem.* **283,** 5677–5684
16. Mizutani, Y., Kihara, A., and Igarashi, Y. (2006) LASS3 (longevity assurance homologue 3) is a mainly testis-specific (dihydro)ceramide synthase with relatively broad substrate specificity. *Biochem. J.* **398,** 531–538
17. Zhao, L., Spassieva, S. D., Jucius, T. J., Shultz, L. D., Shick, H. E., Macklin, W. B., Hannun, Y. A., Obeid, L. M., and Ackerman, S. L. (2011) A deficiency of ceramide biosynthesis causes cerebellar Purkinje cell neurodegeneration and lipofuscin accumulation. *PLoS Genet.* **7,** e1002063
18. Lee, E. C., Yu, D., Martinez de Velasco, J., Tessarollo, L., Swing, D. A., Court, D. L., Jenkins, N. A., and Copeland, N. G. (2001) A highly efficient *Escherichia coli*-based chromosome engineering system adapted for recombinogenic targeting and subcloning of BAC DNA. *Genomics* **73,** 56–65
19. Buchholz, F., Angrand, P. O., and Stewart, A. F. (1998) Improved properties of FLP recombinase evolved by cycling mutagenesis. *Nat. Biotechnol.* **16,** 657–662
20. Magin, T. M., McWhir, J., and Melton, D. W. (1992) A new mouse embryonic stem cell line with good germ line contribution and gene targeting frequency. *Nucleic Acids Res.* **20,** 3795–3796
21. Nagy, A., Gertsenstein, M., Vintersten, K., and Behringer, R. (2003) *Manipulating the Mouse Embryo*, 3rd Ed., pp. 476–480, Cold Spring Harbor Laboratory, Cold Spring Harbor, NY
22. Sambrook, J., and Russel, D. W. (2001) *Molecular Cloning: A Laboratory Manual*, 3rd Ed., pp. 7.31–7.34, Cold Spring Harbor Laboratory, Cold Spring Harbor, NY
23. Maxeiner, S., Dedek, K., Janssen-Bienhold, U., Ammermüller, J., Brune, H., Kirsch, T., Pieper, M., Degen, J., Krüger, O., Willecke, K., and Weiler, R. (2005) Deletion of connexin45 in mouse retinal neurons disrupts the rod/cone signaling pathway between AII amacrine and ON cone bipolar cells and leads to impaired visual transmission. *J. Neurosci.* **25,** 566–576
24. Hanauer, A., and Mandel, J. L. (1984) The glyceraldehyde 3 phosphate dehydrogenase gene family: structure of a human cDNA and of an X chromosome linked pseudogene; amazing complexity of the gene family in mouse. *EMBO J.* **3,** 2627–2633
25. Imgrund, S., Hartmann, D., Farwanah, H., Eckhardt, M., Sandhoff, R., Degen, J., Gieselmann, V., Sandhoff, K., and Willecke, K. (2009) Adult ceramide synthase 2 (CERS2)-deficient mice exhibit myelin sheath defects, cerebellar degeneration, and hepatocarcinomas. *J. Biol. Chem.* **284,** 33549–33560
26. Momoi, T., Ando, S., and Magai, Y. (1976) High resolution preparative column chromatographic system for gangliosides using DEAE-Sephadex and a new porous silica, Iatrobeads. *Biochim. Biophys. Acta* **441,** 488–497
27. Williams, M. A., and McCluer, R. H. (1980) The use of Sep-Pak C18 cartridges during the isolation of gangliosides. *J. Neurochem.* **35,** 266–269
28. Wewer, V., Dombrink, I., vom Dorp, K., and Dörmann, P. (2011) Quantification of sterol lipids in plants by quadrupole time-of-flight mass spectrometry. *J. Lipid Res.* **52,** 1039–1054
29. Welti, R., Li, W., Li, M., Sang, Y., Biesiada, H., Zhou, H. E., Rajashekar, C. B., Williams, T. D., and Wang, X. (2002) Profiling membrane lipids in plant stress responses. Role of phospholipase Dα in freezing-induced lipid changes in *Arabidopsis*. *J. Biol. Chem.* **277,** 31994–32002
30. Jennemann, R., Sandhoff, R., Langbein, L., Kaden, S., Rothermel, U., Gallala, H., Sandhoff, K., Wiegandt, H., and Gröne, H. J. (2007) Integrity and barrier function of the epidermis critically depend on glucosylceramide synthesis. *J. Biol. Chem.* **282,** 3083–3094
31. Sandhoff, R., Geyer, R., Jennemann, R., Paret, C., Kiss, E., Yamashita, T., Gorgas, K., Sijmonsma, T. P., Iwamori, M., Finaz, C., Proia, R. L., Wiegandt, H., and Gröne, H. J. (2005) Novel class of glycosphingolipids involved in male fertility. *J. Biol. Chem.* **280,** 27310–27318
32. Sandhoff, R., Hepbildikler, S. T., Jennemann, R., Geyer, R., Gieselmann, V., Proia, R. L., Wiegandt, H., and Grone, H. J. (2002) Kidney sulfatides in mouse models of inherited glycosphingolipid disorders: determination by nano-electrospray ionization tandem mass spectrometry. *J. Biol. Chem.* **277,** 20386–20398
33. Dere, E., De Souza-Silva, M. A., Frisch, C., Teubner, B., Söhl, G., Willecke, K., and Huston, J. P. (2003) Connexin30-deficient mice show increased emotionality and decreased rearing activity in the open-field along with neurochemical changes. *Eur. J. Neurosci.* **18,** 629–638
34. Zheng-Fischhöfer, Q., Schnichels, M., Dere, E., Strotmann, J., Loscher, N., McCulloch, F., Kretz, M., Degen, J., Reucher, H., Nagy, J. I., Peti-Peterdi, J., Huston, J. P., Breer, H., and Willecke, K. (2007) Characterization of con-

nexin30.3-deficient mice suggests a possible role of connexin30.3 in olfaction. *Eur. J. Cell Biol.* **86,** 683–700
35. Zlomuzica, A., Tress, O., Binder, S., Rovira, C., Willecke, K., and Dere, E. (2012) Changes in object recognition and anxiety-like behaviour in mice expressing a cx47 mutation that causes Pelizaeus-Merzbacher-like disease. *Dev. Neurosci.* **34,** 277–287
36. Zlomuzica, A., Viggiano, D., De Souza Silva, M. A., Ishizuka, T., Gironi Carnevale, U. A., Ruocco, L. A., Watanabe, T., Sadile, A. G., Huston, J. P., and Dere, E. (2008) The histamine H1-receptor mediates the motivational effects of novelty. *Eur. J. Neurosci.* **27,** 1461–1474
37. Bevins, R. A., and Besheer, J. (2005) Novelty reward as a measure of anhedonia. *Neurosci. Biobehav. Rev.* **29,** 707–714
38. Blatter, K., and Schultz, W. (2006) Rewarding properties of visual stimuli. *Exp. Brain Res.* **168,** 541–546
39. Rankin, C. T., Bunton, T., Lawler, A. M., and Lee, S. J. (2000) Regulation of left-right patterning in mice by growth/differentiation factor-1. *Nat. Genet.* **24,** 262–265
40. Sudarov, A., and Joyner, A. L. (2007) Cerebellum morphogenesis: the foliation pattern is orchestrated by multi-cellular anchoring centers. *Neural Dev.* **2,** 26
41. Chiavegatto, S., Sun, J., Nelson, R. J., and Schnaar, R. L. (2000) A functional role for complex gangliosides: motor deficits in GM2/GD2 synthase knockout mice. *Exp. Neurol.* **166,** 227–234
42. Niimi, K., Nishioka, C., Miyamoto, T., Takahashi, E., Miyoshi, I., Itakura, C., and Yamashita, T. (2011) Impairment of neuropsychological behaviors in ganglioside GM3-knockout mice. *Biochem. Biophys. Res. Commun.* **406,** 524–528
43. Tajima, O., Egashira, N., Ohmi, Y., Fukue, Y., Mishima, K., Iwasaki, K., Fujiwara, M., Inokuchi, J., Sugiura, Y., Furukawa, K., and Furukawa, K. (2009) Reduced motor and sensory functions and emotional response in GM3-only mice: emergence from early stage of life and exacerbation with aging. *Behav. Brain Res.* **198,** 74–82
44. Rath, A., Glibowicka, M., Nadeau, V. G., Chen, G., and Deber, C. M. (2009) Detergent binding explains anomalous SDS-PAGE migration of membrane proteins. *Proc. Natl. Acad. Sci. U.S.A.* **106,** 1760–1765
45. Becker, I., Wang-Eckhardt, L., Yaghootfam, A., Gieselmann, V., and Eckhardt, M. (2008) Differential expression of (dihydro)ceramide synthases in mouse brain: oligodendrocyte-specific expression of CerS2/Lass2. *Histochem. Cell Biol.* **129,** 233–241
46. Pewzner-Jung, Y., Park, H., Laviad, E. L., Silva, L. C., Lahiri, S., Stiban, J., Erez-Roman, R., Brügger, B., Sachsenheimer, T., Wieland, F., Prieto, M., Merrill, A. H., Jr., and Futerman, A. H. (2010) A critical role for ceramide synthase 2 in liver homeostasis: I. alterations in lipid metabolic pathways. *J. Biol. Chem.* **285,** 10902–10910
47. Laviad, E. L., Kelly, S., Merrill, A. H., Jr., and Futerman, A. H. (2012) Modulation of ceramide synthase activity via dimerization. *J. Biol. Chem.* **287,** 21025–21033
48. Zheng, W., Kollmeyer, J., Symolon, H., Momin, A., Munter, E., Wang, E., Kelly, S., Allegood, J. C., Liu, Y., Peng, Q., Ramaraju, H., Sullards, M. C., Cabot, M., and Merrill, A. H., Jr. (2006) Ceramides and other bioactive sphingolipid backbones in health and disease: lipidomic analysis, metabolism and roles in membrane structure, dynamics, signaling and autophagy. *Biochim. Biophys. Acta* **1758,** 1864–1884
49. Merrill, A. H., Jr. (1983) Characterization of serine palmitoyltransferase activity in Chinese hamster ovary cells. *Biochim. Biophys. Acta* **754,** 284–291
50. Sun, J., Shaper, N. L., Itonori, S., Heffer-Lauc, M., Sheikh, K. A., and Schnaar, R. L. (2004) Myelin-associated glycoprotein (Siglec-4) expression is progressively and selectively decreased in the brains of mice lacking complex gangliosides. *Glycobiology* **14,** 851–857
51. Montag, D., Giese, K. P., Bartsch, U., Martini, R., Lang, Y., Blüthmann, H., Karthigasan, J., Kirschner, D. A., Wintergerst, E. S., and Nave, K. A. (1994) Mice deficient for the myelin-associated glycoprotein show subtle abnormalities in myelin. *Neuron* **13,** 229–246
52. Watanabe, S., Endo, S., Oshima, E., Hoshi, T., Higashi, H., Yamada, K., Tohyama, K., Yamashita, T., and Hirabayashi, Y. (2010) Glycosphingolipid synthesis in cerebellar Purkinje neurons: roles in myelin formation and axonal homeostasis. *Glia* **58,** 1197–1207
53. Ohmi, Y., Tajima, O., Ohkawa, Y., Yamauchi, Y., Sugiura, Y., Furukawa, K., and Furukawa, K. (2011) Gangliosides are essential in the protection of inflammation and neurodegeneration via maintenance of lipid rafts: elucidation by a series of ganglioside-deficient mutant mice. *J. Neurochem.* **116,** 926–935
54. Blank, M. C., Grinberg, I., Aryee, E., Laliberte, C., Chizhikov, V. V., Henkelman, R. M., and Millen, K. J. (2011) Multiple developmental programs are altered by loss of Zic1 and Zic4 to cause Dandy-Walker malformation cerebellar pathogenesis. *Development* **138,** 1207–1216
55. Teigler, A., Komljenovic, D., Draguhn, A., Gorgas, K., and Just, W. W. (2009) Defects in myelination, paranode organization and Purkinje cell innervation in the ether lipid-deficient mouse cerebellum. *Hum Mol. Genet.* **18,** 1897–1908
56. Kim, Y. S., Harry, G. J., Kang, H. S., Goulding, D., Wine, R. N., Kissling, G. E., Liao, G., and Jetten, A. M. (2010) Altered cerebellar development in nuclear receptor TAK1/TR4 null mice is associated with deficits in $GLAST^+$ glia, alterations in social behavior, motor learning, startle reactivity, and microglia. *Cerebellum* **9,** 310–323
57. Simpson, M. A., Cross, H., Proukakis, C., Priestman, D. A., Neville, D. C., Reinkensmeier, G., Wang, H., Wiznitzer, M., Gurtz, K., Verganelaki, A., Pryde, A., Patton, M. A., Dwek, R. A., Butters, T. D., Platt, F. M., and Crosby, A. H. (2004) Infantile-onset symptomatic epilepsy syndrome caused by a homozygous loss-of-function mutation of GM3 synthase. *Nat. Genet.* **36,** 1225–1229
58. Di Pardo, A., Maglione, V., Alpaugh, M., Horkey, M., Atwal, R. S., Sassone, J., Ciammola, A., Steffan, J. S., Fouad, K., Truant, R., and Sipione, S. (2012) Ganglioside GM1 induces phosphorylation of mutant huntingtin and restores normal motor behavior in Huntington disease mice. *Proc. Natl. Acad. Sci. U.S.A.* **109,** 3528–3533
59. Contreras, F. X., Ernst, A. M., Haberkant, P., Björkholm, P., Lindahl, E., Gönen, B., Tischer, C., Elofsson, A., von Heijne, G., Thiele, C., Pepperkok, R., Wieland, F., and Brügger, B. (2012) Molecular recognition of a single sphingolipid species by a protein's transmembrane domain. *Nature* **481,** 525–529